Volume 23
Number 29
7 August 2021
Pages 15389–15798

PCCP

Physical Chemistry Chemical Physics

rsc.li/pccp

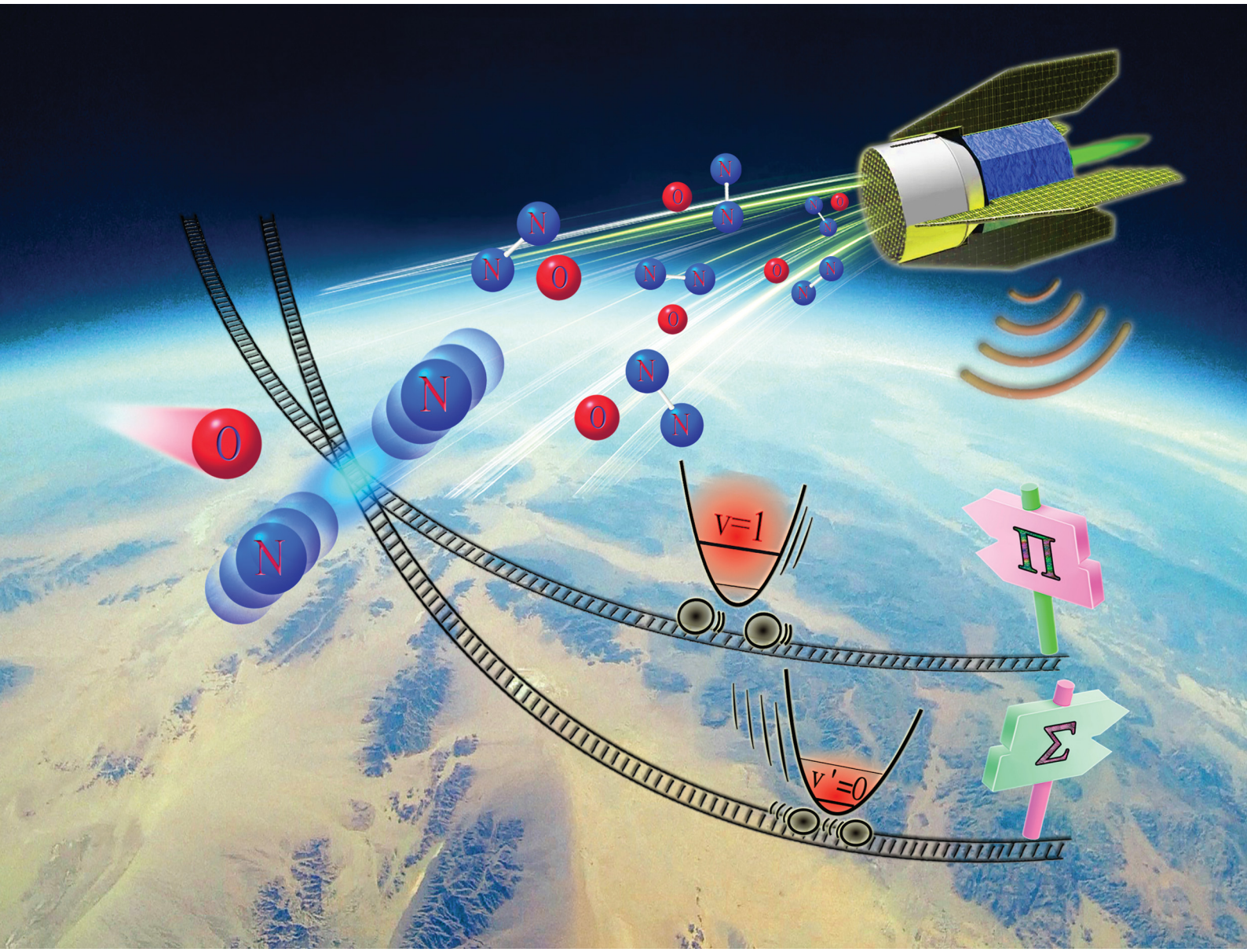

ISSN 1463-9076

ROYAL SOCIETY OF CHEMISTRY

COMMUNICATION

Cecilia Coletti *et al.*

Reconciling experimental and theoretical vibrational deactivation in low-energy O + N_2 collisions

PCCP

COMMUNICATION

View Article Online
View Journal | View Issue

Cite this: *Phys. Chem. Chem. Phys.*, 2021, **23**, 15475

Received 4th May 2021,
Accepted 1st June 2021

DOI: 10.1039/d1cp01976g

rsc.li/pccp

Reconciling experimental and theoretical vibrational deactivation in low-energy O + N_2 collisions†

Qizhen Hong, [ab] Massimiliano Bartolomei, [c] Fabrizio Esposito, [d] Cecilia Coletti, *[e] Quanhua Sun [ab] and Fernando Pirani [f]

Molecular dynamics calculations of inelastic collisions of atomic oxygen with molecular nitrogen are known to show orders of magnitude discrepancies with experimental results in the range from room temperature to many thousands of degrees Kelvin. In this work, we have achieved an unprecedented quantitative agreement with experiments even at low temperature, by including a non-adiabatic treatment involving vibronic states on newly developed potential energy surfaces. This result paves the way for the calculation of accurate and detailed databases of vibrational energy exchange rates for this collisional system. This is bound to have an impact on air plasma simulations under a wide range of conditions and on the development of Very Low Earth Orbit (VLEO) satellites, operating in the low thermosphere, objects of great technological interest due to their potential at a competitive cost.

Reactive, inelastic and dissociation processes in molecular collisions of air species play a crucial role in the accurate modelization of air plasmas, which include combustion processes,[1] planetary entry problems,[2] electrical discharges,[3] atmospheric kinetics,[4,5] and plasma medicine.[6] In these systems, it is common to find strong non-equilibrium conditions in different molecular degrees of freedom, which impose the adoption of detailed state-to-state models[7] for the comprehension and control of phenomena of wide technological interest. In these models, the required input data may come from experiments and/or from theoretical calculations. In the first case it is quite unlikely to extract all the needed data, considering the large total energy ranges normally required. As a consequence, detailed computations of (ro)vibrationally detailed kinetic data using molecular dynamics methods from accurate potential energy surfaces (PES), describing the interactions in the collisions, become utterly necessary. The results of these calculations can then be compared with the experimental data in the usually available intervals, in order to assess their accuracy. Among air species processes, one case of special interest is represented by the collisions of atomic oxygen with molecular nitrogen. The quite common presence of atomic oxygen in air plasmas is due to the fact that the molecular oxygen dissociation threshold is much lower than that for nitrogen. Atomic oxygen is also found in the low thermosphere, a region between 90 and 250 km of altitude, which is of great relevance for future satellite constellations, where UV radiation from the Sun dissociates O_2, so that the most abundant species are precisely O and N_2. The accurate knowledge of their interactions, determining the low temperature range (300–1000 K) behavior, is urgent, in view of the development of Very Low Earth Orbit (VLEO) satellites with air-breathing electric propulsion systems,[8–11] capable in principle of endless operation without a propellant tank. As a consequence, a detailed study on O + N_2 interactions is currently of strategic importance. The modelling of non-equilibrium operating conditions in shock waves, for instance, is very sensitive to vibrational relaxation rates, crucial to predict the correct vibrational temperature and relaxation times.[12] Collisions of O with $N_2(v)$ in turn generate excited $N_2(v')$ molecules in an inelastic process, or $NO(v')$ + N reaction, or N_2 dissociation. Recent computations of reaction and dissociation rates appear to be in good agreement with what is known about these processes,[13–16] but the experimental results for the O + $N_2(1)$ → O + $N_2(0)$ inelastic process in the 300–4500 K interval, where the system is mainly characterized by non-reactive collisions, have not yet been reproduced using theoretical calculations, which present severe under-estimations (of orders of magnitude) at room temperature,[13,16,17] and important over-[16,17] or under-estimations[13] at temperatures higher than 1000 K.

[a] *State Key Laboratory of High Temperature Gas Dynamics, Institute of Mechanics, Chinese Academy of Sciences, 100190 Beijing, China*
[b] *School of Engineering Science, University of Chinese Academy of Sciences, Beijing 100049, China*
[c] *Instituto de Física Fundamental-CSIC, C/Serrano 123, Madrid, Spain*
[d] *Consiglio Nazionale delle Ricerche, Istituto per la Scienza e Tecnologia dei Plasmi, Sede Secondaria di Bari, via Amendola 122/D 70126 Bari, Italy*
[e] *Dipartimento di Farmacia, Università G. d'Annunzio Chieti-Pescara, via dei Vestini, 66100 Chieti, Italy. E-mail: ccoletti@unich.it*
[f] *Dipartimento di Chimica, Biologia e Biotecnologie, Università di Perugia, via Elce di Sotto 8, 06123 Perugia, Italy*

† Electronic supplementary information (ESI) available. See DOI: 10.1039/d1cp01976g

The basic ingredient needed to properly investigate the elementary processes promoted by collisions is the accurate characterization of the interaction potentials driving the molecular dynamics. The evolution of the inelastic scattering processes, particularly at low temperature, is known to be strongly dependent on the long range region of the potential, a part of the PES which is seldom well characterized. Therefore, the present investigation was initially motivated by the need of an accurate non-reactive PES, providing the best possible description at long and medium range, and likely to give a physically meaningful insight on inelastic collisional events. Such potential in turn should be expressed in a simple form capable to represent the full space of relative configurations of the involved partners. It should furthermore describe the formation, by two-body collisions, of weakly bound adducts, representing the precursor states of further basic processes. This might still be a tough challenge for potentials exclusively based on *ab initio* computations: a very high level of theory is required to evaluate the small interaction energies of weakly non-covalently bound systems and the number of points required to fully cover all possible long range regions could easily become prohibitive.

We have thus represented the multidimensional PES for $O(^3P_J)$–$N_2(^1\Sigma_g^+)$ in analytical form, by taking into account that at intermediate and large intermolecular distances R the interaction is determined by the balance between van der Waals (vdW) forces and other contributions, deriving from different reciprocal alignments of N_2 molecular axis and of the half-filled orbitals of $O(^3P_J)$ atom with respect to R.[19] J = 2,1,0 represent the total electronic angular momentum states of the oxygen atom, which, for a plasma at $T \geq 1000$ K, are statistically populated in a 5 : 3 : 1 ratio. In the following, we will use the shorter notation $O(^3P)$ for simplicity. Only $O(^3P)$ oxygen atoms are considered here: all experimental determinations referred to in the present Communication are indeed obtained in the absence[18,20,21] or with a negligible presence[22] of $O(^1D)$ atoms.

Strength and anisotropy of the interaction contributions other than V_{vdW} are mainly dependent on the electrostatic quadrupole–quadrupole component (V_{el}), arising from the non-spherical electronic charge distribution of both partners, and on the selective charge transfer (CT) effects (V_{ct}) in the perturbation limit emerging in systems involving high electron affinity open shell atoms, as is the case for $O(^3P)$.[19,23] Accordingly, we have defined the total interaction V_{tot} as

$$V_{tot} = V_{vdW} + V_{ct} + V_{el} \quad (1)$$

Particular effort has been addressed to represent each of the contributions through simple analytical formulae depending on few and physically meaningful parameters, leading to a correct representation of the interaction in the full space of the relative configurations.

V_{el} is given by the canonical expression of quadrupole–quadrupole interactions, whereas the sum of the first two components, $V_{vdW} + V_{ct}$, has been formulated as the combination of pair interactions between $O(^3P)$ and each N atom of the N_2 molecule, described by an Improved Lennard Jones (ILJ) function,[24] whose details are given in the ESI.† Zero order values of the parameters involved in the ILJ expression have been estimated from the polarizability of the O atom (0.8 Å^3) and the effective component of that of each N atom (0.9 Å^3) within N_2. According to the ample phenomenology of $O(^3P)$ interacting with closed shell partners,[23,25] two different types of interaction can be distinguished: the oxygen atom approaching N_2 with one of the half-filled p orbitals aligned parallel to the intermolecular distance R, leading to the formation of the $^3\Pi$ state (electronic molecular quantum number Λ = 1), and that with the oxygen atom approaching with the only filled orbital aligned along R, leading to a $^3\Sigma$ state (Λ = 0).[23] This diversification accounts for the contribution of CT, which was found to selectively stabilize the states of Π symmetry.[25]

The zero order parameters were then fine tuned exploiting the simultaneous comparison of the predicted intermolecular interaction with the results of *ab initio* calculations, and its ability to reproduce experimental total cross sections, leading to the values reported in Table S1 in the ESI.†

The left panel of Fig. 1 reports the two $O(^3P)$–$N_2(^1\Sigma_g^+)$ ground $^3\Pi$ and first excited $^3\Sigma$ (lying asymptotically 28.1 meV above the $^3\Pi$ state and directly correlating with the excited spin orbit level $^3P_0$[23,25]) PESs as a function of the intermolecular distance R for the two limiting orientations (parallel and perpendicular) of the diatom (at its equilibrium distance) approaching the oxygen atom.

The figure also shows the *ab initio* energy values obtained at the CCSD(T)/CBS level of theory. Note that, in the case of the perpendicular orientation for the $^3\Pi$ state, *ab initio* data provide two non-coincident sets (red circles) for the potential energies, depending on the two different orientations of the fully occupied p orbital of the oxygen atom with respect to the diatom. The two sets are degenerate under the $C_{\infty v}$ (parallel)

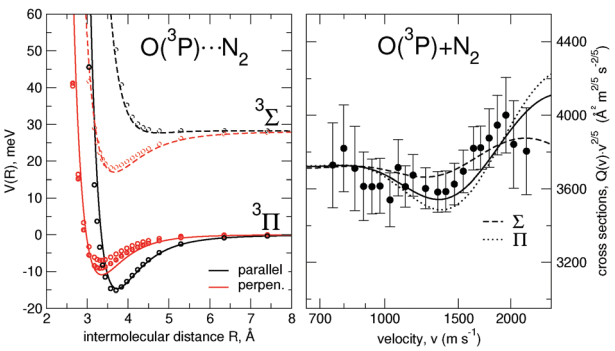

Fig. 1 Left panel: Intermolecular potentials for the interaction between $O(^3P)$ and $N_2(^1\Sigma_g^+)$ as a function of the distance R between the oxygen atom and the center of mass of the N_2 molecule at its equilibrium distance. Black and red lines are obtained through the present analytical PES and correspond to the parallel and perpendicular orientations, respectively, of N_2 with respect to the oxygen atom. Symbols, colored accordingly, correspond to the *ab initio* calculations carried out at the CCSD(T)/CBS level of theory. Right panel: Integral cross sections for the $O(^3P)$ + $N_2(^1\Sigma_g^+)$ collisions as a function of the selected atom beam velocity v. Full circles correspond to experimental data from the Perugia laboratory,[18] while curves correspond to calculations on the present analytical PESs using an IOS approximation: the dotted curve is obtained by using the $^3\Pi$ surface, the dashed one by the $^3\Sigma$ PES and the full black line corresponds to cross sections obtained by averaging the results on the two PESs according to their statistical 2 : 1 population.

configuration of the system and split in the C_{2v} (perpendicular) configuration, corresponding to the $^3B_2$ and $^3B_1$ symmetries. These symmetries in turn correlate with the $^3A'$ and $^3A''$ states of the more general C_s configuration. Because the difference in energy between these two kinds of interaction is small and tends to zero for both small and large R values (and does not exist in the $^3\Sigma$ state), we simplified the present model by only considering an average contribution of the $^3A'$ and $^3A''$ states, collectively indicating it as $^3\Pi$ PES.

Fig. 1 (right panel) reports the experimental total cross sections Q, measured as a function of the selected velocity v of projectile O atoms and under single collision conditions with the target N_2 molecules.[18] The data have been plotted as $Q(v)\cdot v^{2/5}$ to emphasize the quantum interference effects, observable as an oscillatory pattern in the v dependence of the measured $Q(v)$. The average $Q(v)$ values directly probe the strength of the long range average dispersion attraction, while the extrema position and the frequency of the oscillating pattern give unique information on the depth and on the minimum location of the potential well, which occur at intermediate separation distances and are determined by a critical balance of attraction and repulsion. The total cross sections calculated on both $^3\Pi$ and $^3\Sigma$ PESs are also displayed in the figure, together with their combination, weighted by the degeneracy ratio 2 : 1, according to the statistical population of the oxygen fine levels in the atomic beam[18] (Experimental and Computational Details in the ESI†). The latter is shown to reproduce the relevant behavior of the experimental data within their uncertainty.

The present non-reactive PESs, with the inclusion of the intramolecular potential for N_2 (here taken as the Morse potential) can be used for the calculation of the rates of the inelastic vibrational relaxation processes involving vibrationally excited N_2 molecules at temperatures lower than 10 000 K, where the influence of the reactive channels is still small. The case of the vibrational relaxation of $N_2(v = 1)$ upon collision with $O(^3P)$, for which experimental results in the temperature range 300–4500 K are available[20–22] (details can be found in ESI†), is particularly intriguing because quasi-classical trajectory (QCT) calculations performed on most of the existing PESs,[14,26,27] available for the $^3A'$ and $^3A''$ states of this system, are known to underestimate[13,28] the experimental rate coefficients of 1–2 orders of magnitude at $T \approx$ 2000–4000 K and of 3–4 orders of magnitude at lower temperature (see Fig. 2). At very low temperatures (less than 500–700 K), QCT calculations are not able to foresee any probability of V–T energy exchange. This is expected, because vibrational inelastic energy transfer can be a classically forbidden process.[29] In short, the classical final vibration is only slightly different from the initial one for sufficiently low energy so that the QCT binning becomes unable to detect a small, but non-zero, result different from the elastic one.[13] In order to avoid this effect, which could affect the results independently on the PES quality, we used a mixed quantum-classical (QC) method,[30–32] whereby the N_2 vibration is described by quantum mechanics and the other degrees of freedom classically (details are given in ESI†). We used the QC method also in combination with Gamallo *et al.* PES,[26] for which QCT calculations are available,[13]

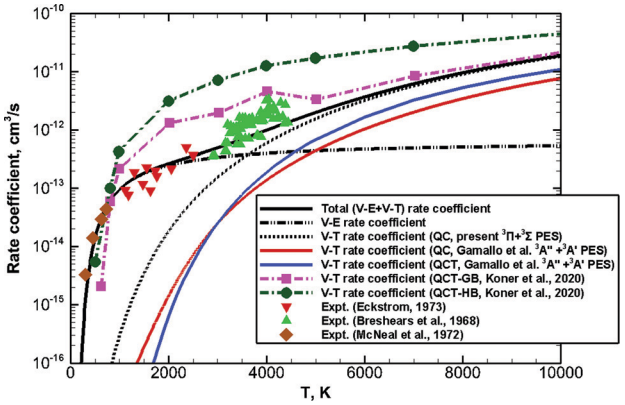

Fig. 2 Rate coefficients for vibrational relaxation upon $O(^3P)$–$N_2(^1\Sigma_g^+)(v = 1)$ collision as a function of temperature. Experimental data by Eckstrom[20] (red down triangles), by Breshears and Bird[21] (green up triangles) and by McNeal *et al.*[22] (brown diamonds) are reported together with QCT[13] (blue solid line) and QC (red solid line) V–T rate coefficients computed on Gamallo *et al.* PES,[26] on Koner *et al.* PES[16,17] by a QCT method associated with a standard Histogram Binning (dark green dash-dot line with circles) or a Gaussian Binning procedure (pink dash-dot line with squares), and on the present $^3\Pi$ and $^3\Sigma$ surfaces (2 : 1 averaged) using a QC method (black dotted line). Rate coefficients for the non-adiabatic vibro–electronic (V–E) transition between $^3\Pi(v = 1)$ and $^3\Sigma(v = 0)$ calculated according to the LZ approach are shown using a black dashed-dotted line. The weighted sum of the present V–T and V–E rate coefficients, representing the total vibrational relaxation rate, is shown using a solid black line.

allowing for the quantification of the effect of the QC dynamical treatment over the QCT one, as also reported in Fig. 2 and Fig. S1 in the ESI.† As expected, QC and QCT values are close at $T \geq$ 3000 K, whereas QC results grow larger than the QCT ones as temperature decreases.

Fig. 2 also reports the rate coefficients calculated on the present ground $^3\Pi$ and excited $^3\Sigma$ PESs averaged according to their statistical 2 : 1 population. Rate coefficients calculated separately on the $^3\Pi$ and on the $^3\Sigma$ potentials can be found in Fig. S2 in the ESI.† Only those obtained on the $^3\Pi$ PES can be directly compared to those calculated on the $^3A'$ and $^3A''$ PESs. The new PESs, and in particular the $^3\Pi$ one, provide sensibly higher (*ca.* one order of magnitude at $T \geq$ 2000 K and larger as the temperature decreases) rate coefficients than Gamallo *et al.* PES,[26] whereas the standard QCT values calculated with the recent Koner *et al.* PES[16,17] are up to three orders of magnitude larger in the 1000–4000 K interval, rapidly dropping down at lower temperature. Compared to the experimental vibrational relaxation data, the present results are only slightly smaller in the range of 3000–4000 K, but the difference, strongly growing as temperature decreases, rises up to 2–3 orders of magnitude at $T \leq$ 3000 K. This behavior and a closer look at the $^3\Pi$ and $^3\Sigma$ PESs point out that the reason for such apparent discrepancy must have a different origin.

As suggested by Nikitin and Umanski,[33] the unusually high vibrational relaxation rates for $N_2(v = 1)$ when colliding with $O(^3P)$ at low T are due to the open shell nature of oxygen leading to the non-adiabatic vibro–electronic (V–E) energy transfer[34,35] which takes place at the crossing between the $^3\Pi$ and $^3\Sigma$ vibronic surfaces.

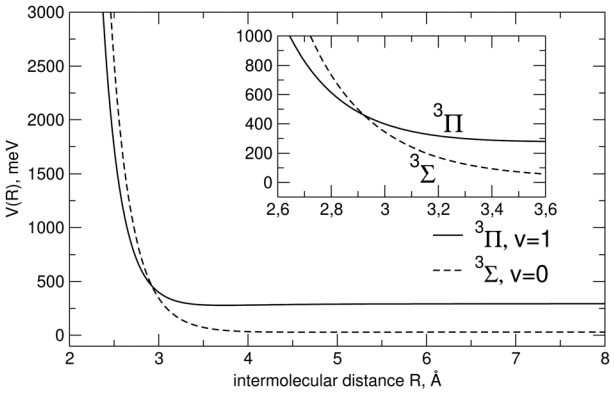

Fig. 3 Potential curves for the O(^{3}P)–N$_2$($^1\Sigma_g^+$) interaction with N$_2$ molecular axis oriented along the intermolecular distance. In order to determine the main features between the vibronic states responsible for molecular relaxation, the molecule is assumed in the first excited v = 1 vibration level for the $^3\Pi$ state, while for the $^3\Sigma$ state v = 0 is considered.

Indeed, as shown in Fig. 3 for the collinear $C_{\infty v}$ configuration, expected to be the most effective for inelastic events promoted by vibronic couplings, the $^3\Pi(v = 1)$ and the $^3\Sigma(v = 0)$ PESs cross at R_c = 2.922 Å where the potential energy is E_x = 0.1666 eV in the entrance channel, a value obtained as the difference between the energy at the crossing E_c, 0.4592 eV, and the vibrational quantum of energy for N$_2$(v = 1), 0.2926 eV.

The detailed description of the two PESs gives us the possibility to quantitatively evaluate the *V–E* contribution to the vibrational quenching rate, according to the Landau–Zener (LZ) approach.[36–38] *V–E* rate coefficients are reported as a function of temperature in Fig. 2: they strongly increase with temperature to reach a plateau at $T \geq 2000$ K. At temperatures lower than 2000 K, the *V–E* rates are higher than the *V–T* ones, and the overall vibrational quenching rate is thus mainly determined by the vibronic energy transfer process. This is very clearly indicated by the calculated total relaxation rate (Fig. 2), obtained as the sum of the *V–T* contribution and the *V–E* one, the latter multiplied by 2/3 as it only occurs on the $^3\Pi$ PES. The excellent agreement between calculations and experimental data (Table. S3 and Fig. S3 in ESI†), both at low (where *V–E* energy transfer dominates) and high (where *V–T* rate coefficients prevail) temperatures, represents a strong indication that the apparent theory–experiment disagreement is in fact the result of the neglection of one important physical contribution to the removal of excited nitrogen molecules. The relative efficiency of the *V–T* and *V–E* processes to the vibrational quenching of N$_2$(v = 1) at different ranges of collisional energy can be better appreciated by comparing their corresponding excitation functions reported in Fig. S4 in the ESI.† Note that the non-adiabatic transition between the reactants triplet PESs and the N_2O singlet,[39] occurring at higher energies (with a threshold around 1 eV), might be responsible for the slight difference between the present relaxation rate and experimental data in the temperature range over 3500 K.

The matching between the calculated and experimental values of the total relaxation rates prompts us to investigate where the discrepancy between the *V–T* rate coefficients computed on the present PES and those available in the literature (Fig. 2) arises from. To this aim, Fig. 4 reports the potential energy as a function of the intermolecular distance R for the $^3A'$ and $^3A''$ PESs of Gamallo *et al.*[26] and those of Koner *et al.*[17] and the present $^3\Pi$ for the parallel configuration, the most relevant for the processes considered here. We recall that $^3A'$ and $^3A''$ should be degenerate for the parallel (collinear) configuration and asymptotically for all configurations.

Fig. 4 shows that in fact the $^3A''$ and $^3A'$ PESs of ref. 26 only coincide at long range; the short range divergence probably due to the interpolation procedure which, by mixing the $C_{\infty v}$ collinear points with diverse symmetry non-degenerate neighbouring points ($^3A''$ and $^3A'$ differently correlate with the reactive channels), might spuriously remove the degeneracy. The qualitative behavior of both PESs however is similar to the new $^3\Pi$ surface (falling below and above, respectively) at long range, with the *V–T* rates calculated on the $^3A'$ slightly larger (Fig. S1 in ESI†). Both $^3A''$ and $^3A'$ surfaces at short range are less repulsive than $^3\Pi$ potential which might be the reason why the *V–T* rate coefficients are about one order of magnitude smaller than the presently computed ones.

The $^3A''$ and $^3A'$ PESs of Ref. 16 show the opposite behavior: they practically coincide at short range (up to $R \approx 4.5$ Å), but they diverge at long range, where they both present a high early barrier and a well with a steep attractive side. This repulsive behavior at long interaction distances might be the reason of the very large *V–T* rate coefficients calculated on these PESs. Similar differences can be found for the perpendicular configuration as shown in Fig. S5 in the ESI.†

The present investigation, providing a detailed characterization of intermediate and asymptotic regions of the O(^{3}P)–N$_2$ interaction, casts light on the presence of crossings between potential energy surfaces of different electronic symmetries where vibronic non-adiabatic events are triggered. Although as early as 1972 vibrational-electronic energy transfer was suggested to be crucial

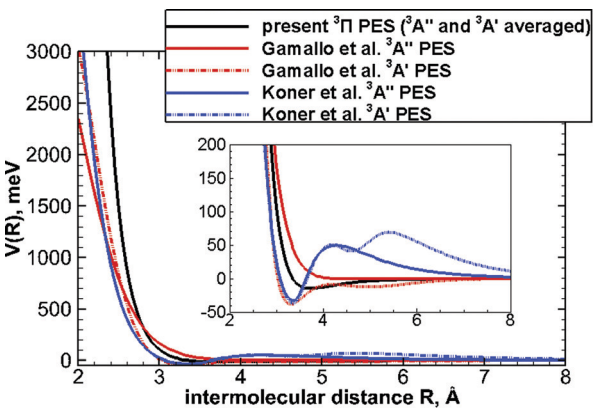

Fig. 4 Behavior of different potential energy surfaces as a function of the intermolecular distance R for the collinear (or parallel) configuration, corresponding to the $C_{\infty v}$ symmetry. The present $^3\Pi$ PES is reported as a solid black line, the Gamallo *et al.*[26] $^3A''$ and $^3A'$ are the red solid and dashed lines, respectively, and the Koner *et al.*[17] $^3A''$ and $^3A'$ are the blue solid and dashed lines, respectively.

for vibrational quenching when oxygen atoms are involved, this contribution has been neither considered nor evaluated previously. Therefore, in addition to the canonical vibration-translation inelasticity, vibration-electronic energy transfers can also be effectively promoted by collisions. One crucial point here is that the two types of events emerge in different ranges of gaseous-mixture temperature. Note that the significance of these findings is not limited to $O(^3P)$–N_2 collisions; they are of broad interest for the control of elastic and inelastic elementary processes occurring in several plasmas where open shell O atoms are involved in the collision with many other molecular partners.

Conflicts of interest

There are no conflicts to declare.

Acknowledgements

Q. H. and Q. S. acknowledge financial support from the Strategic Priority Research Program of Chinese Academy of Sciences (Grant No. XDA17030100) and the National Natural Science Foundation of China through grants 11372325 and 91116013. M. B. acknowledges the FIS2017-84391-C2-2-P Spanish grant for funding.

References

1 I. V. Adamovich and W. R. Lempert, *Plasma Phys. Controlled Fusion*, 2015, **57**, 014001.
2 R. Celiberto, I. Armenise, M. Cacciatore, M. Capitelli, F. Esposito, P. Gamallo, R. K. Janev, A. Laganà, V. Laporta, A. Laricchiuta, A. Lombardi, M. Rutigliano, R. Sayós, J. Tennyson and J. M. Wadehra, *Plasma Sources Sci. Technol.*, 2016, **25**, 033004.
3 C. D. Pintassilgo and V. Guerra, *J. Phys. Chem. C*, 2016, **120**, 21184–21201.
4 A. V. Pavlov, *Geomagn. Aeron.*, 2011, **51**, 143–169.
5 V. Yankovsky and E. Vorobeva, *Atmosphere*, 2020, **11**, 116.
6 M. Keidar, *Plasma Sources Sci. Technol.*, 2015, **24**, 033001.
7 M. Capitelli, I. Armenise, E. Bisceglie, D. Bruno, R. Celiberto, G. Colonna, G. D'Ammando, O. De Pascale, F. Esposito, C. Gorse, V. Laporta and A. Laricchiuta, *Plasma Chem. Plasma Process.*, 2012, **32**, 427–450.
8 P. Parodi, D. L. Quang, F. Bariselli, S. Boccelli and T. Magin, *International Conference on Flight vehicles, Aerothermodynamics and Re-entry Missions and Engineering (FAR)*, 2019.
9 A. I. Erofeev, A. P. Nikiforov, G. A. Popov, M. O. Suvorov, S. A. Syrin and S. A. Khartov, *Sol. Syst. Res.*, 2017, **51**, 639–645.
10 M. Leomanni, A. Garulli, A. Giannitrapani and F. Scortecci, *Acta Astronaut.*, 2017, **133**, 444–454.
11 K. Holste, P. Dietz, S. Scharmann, K. Keil, T. Henning, D. Zschätzsch, M. Reitemeyer, B. Nauschütt, F. Kiefer, F. Kunze, J. Zorn, C. Heiliger, N. Joshi, U. Probst, R. Thüringer, C. Volkmar, D. Packan, S. Peterschmitt, K. T. Brinkmann, H.-G. Zaunick, M. H. Thoma, M. Kretschmer, H. J. Leiter, S. Schippers, K. Hannemann and P. J. Klar, *Rev. Sci. Instrum.*, 2020, **91**, 061101.
12 C. Park, *J. Thermophys. Heat Transfer*, 2006, **20**, 689–698.
13 F. Esposito and I. Armenise, *J. Phys. Chem. A*, 2017, **121**, 6211–6219.
14 W. Lin, Z. Varga, G. Song, Y. Paukku and D. G. Truhlar, *J. Chem. Phys.*, 2016, **144**, 024309.
15 H. Luo, M. Kulakhmetov and A. Alexeenko, *J. Chem. Phys.*, 2017, **146**, 074303.
16 D. Koner, J. C. San Vicente Veliz, R. J. Bemish and M. Meuwly, *Phys. Chem. Chem. Phys.*, 2020, **22**, 18488–18498.
17 D. Koner, R. J. Bemish and M. Meuwly, *J. Phys. Chem. A*, 2020, **124**, 6255–6269.
18 B. Brunetti, G. Liuti, E. Luzzatti, F. Pirani and F. Vecchiocattivi, *J. Chem. Phys.*, 1981, **74**, 6734–6741.
19 F. Pirani, G. S. Maciel, D. Cappelletti and V. Aquilanti, *Int. Rev. Phys. Chem.*, 2006, **25**, 165–199.
20 D. J. Eckstrom, *J. Chem. Phys.*, 1973, **59**, 2787–2795.
21 W. D. Breshears and P. F. Bird, *J. Chem. Phys.*, 1968, **48**, 4768–4773.
22 R. McNeal, M. Whitson and G. Cook, *Chem. Phys. Lett.*, 1972, **16**, 507–510.
23 V. Aquilanti, G. Liuti, F. Pirani and F. Vecchiocattivi, *J. Chem. Soc., Faraday Trans. 2*, 1989, **85**, 955–964.
24 F. Pirani, S. Brizi, L. Roncaratti, P. Casavecchia, D. Cappelletti and F. Vecchiocattivi, *Phys. Chem. Chem. Phys.*, 2008, **10**, 5489–5503.
25 V. Aquilanti, R. Candori and F. Pirani, *J. Chem. Phys.*, 1988, **89**, 6157–6164.
26 P. Gamallo, M. González and R. Sayós, *J. Chem. Phys.*, 2003, **119**, 2545–2556.
27 O. Denis-Alpizar, R. J. Bemish and M. Meuwly, *Phys. Chem. Chem. Phys.*, 2017, **19**, 2392–2401.
28 M. V. Ivanov, R. Schinke and G. C. Mcbane, *Mol. Phys.*, 2007, **105**, 1183–1191.
29 W. H. Miller, *J. Chem. Phys.*, 1970, **53**, 3578.
30 G. Billing, *Comput. Phys. Commun.*, 1984, **32**, 45–62.
31 Q. Hong, Q. Sun, M. Bartolomei, F. Pirani and C. Coletti, *Phys. Chem. Chem. Phys.*, 2020, **22**, 9375–9387.
32 Q. Hong, Q. Sun, F. Pirani, M. A. Valentín-Rodríguez, R. Hernández-Lamoneda, C. Coletti, M. I. Hernández and M. Bartolomei, *J. Chem. Phys.*, 2021, **154**, 064304.
33 E. E. Nikitin and S. Y. Umanski, *Faraday Discuss. Chem. Soc.*, 1972, **53**, 7–17.
34 R. Candori, S. Cavalli, F. Pirani, A. Volpi, D. Cappelletti, P. Tosi and D. Bassi, *J. Chem. Phys.*, 2001, **115**, 8888–8898.
35 R. Candori, F. Pirani, D. Cappelletti, P. Tosi and D. Bassi, *Int. J. Mass Spectrom.*, 2003, **223-224**, 499–506.
36 L. D. Landau, *Phys. Z. Sowjetunion*, 1932, **2**, 46–51.
37 C. Zener, *Proc. R. Soc. London*, 1932, **A137**, 696–702.
38 E. C. G. Stückelberg, *Helv. Phys. Acta*, 1932, **5**, 369–423.
39 E. R. Fisher and E. Bauer, *J. Chem. Phys.*, 1972, **57**, 1966.